




Research Article

Open Access



Magnetic-field driven domain wall evolution in rhombohedral magnetostrictive single crystals: a phase-field simulation

Yu-Xin Xu^{1,*}, Ting-Tao Cai^{1,*}, Cheng-Chao Hu¹ , Zhao Zhang¹, Shou-Zhe Dong², Hai-Hua Huang¹, Wei Li¹, Hou-Bing Huang² , Long-Qing Chen³ , Wei-Feng Rao⁴

¹School of Materials Science and Engineering, Liaocheng University, Liaocheng 252000, Shandong, China.

²Advanced Research Institute of Multidisciplinary Science, Beijing Institute of Technology, Beijing 100081, China.

³Department of Materials Science and Engineering, The Pennsylvania State University, University Park, PA 16802, USA.

⁴School of Mechanical Engineering, Qilu University of Technology (Shandong Academy of Sciences), Jinan 250353, China.

*Authors contributed equally.

Correspondence to: Dr. Chengchao Hu, School of Materials Science and Engineering, Liaocheng University, Liaocheng, Shandong 252000, China. E-mail: huchengchao@lcu.edu.cn; Dr. Zhao Zhang, School of Materials Science and Engineering, Liaocheng University, Liaocheng 252000, Shandong, China. E-mail: zhangzhao@lcu.edu.cn

How to cite this article: Xu YX, Cai TT, Hu CC, Zhang Z, Dong SZ, Huang HH, Li W, Huang HB, Chen LQ, Rao WF. Magnetic-field driven domain wall evolution in rhombohedral magnetostrictive single crystals: a phase-field simulation. *Microstructures* 2024;4:2024052. <https://dx.doi.org/10.20517/microstructures.2023.104>

Received: 30 Dec 2023 **First Decision:** 7 Mar 2024 **Revised:** 28 Mar 2024 **Accepted:** 29 Apr 2024 **Published:** 17 Aug 2024

Academic Editor: Jiamian Hu **Copy Editor:** Fangyuan Liu **Production Editor:** Fangyuan Liu

Abstract

Single crystal of $Tb_{0.3}Dy_{0.7}Fe_2$ (Terfenol-D) with a composition close to the pre-transitional rhombohedral side of the ferromagnetic morphotropic phase boundary has demonstrated remarkable magnetostrictive properties, stimulating intensive research interest in the field of magneto-mechanical transducers and actuators. The enhanced magnetoelastic response of $(Tb-Dy)Fe_2$ single crystals has been extensively linked to the structural phase transition and magnetic domain evolution. This research utilized the micromagnetic microelastic phase-field technique to examine the evolution of domain walls in rhombohedral ferromagnetic single crystals of $(Tb-Dy)Fe_2$, which is essential for understanding the magnetostriction “jump” effect. The study involved simulating the creation and development of domains and domain boundaries under a periodic boundary condition that allows for non-zero strain. It was found that the two typical distinct types of domain walls (i.e., 71° and 109°) exhibited disparate responses to the applied magnetic fields. At magnetic field magnitudes below the coercive field, a domain wall broadening mechanism was detected within the 71° domain wall. However, upon surpassing the coercive field, a process of homogeneous magnetization switching ensued, devoid of evident displacement of the 71° domain walls. The magnetization switching effectively elucidated the magnetostriction “jump” effect of the rhombohedral single



© The Author(s) 2024. **Open Access** This article is licensed under a Creative Commons Attribution 4.0 International License (<https://creativecommons.org/licenses/by/4.0/>), which permits unrestricted use, sharing, adaptation, distribution and reproduction in any medium or format, for any purpose, even commercially, as long as you give appropriate credit to the original author(s) and the source, provide a link to the Creative Commons license, and indicate if changes were made.



crystals. The act of sweeping the 109° domain walls resulted in the occurrence of heterogeneous magnetization switching. This study elucidates the evolutionary mechanism of two typical rhombohedral domain walls in response to applied magnetic fields, potentially offering valuable insights into the future design of excellent magnetostrictive materials through domain engineering.

Keywords: Phase-field simulation, ferromagnetic MPB, magnetostriction, domain wall

INTRODUCTION

Giant magnetostrictive materials, i.e., quasi-binary (Tb-Dy)Fe₂ alloys, have attracted considerable attention due to their potential applications as energy conversion components in magneto-mechanical transducers and actuators^[1-6]. During the past decades, efforts have been made to develop an anisotropy compensation system that minimizes magnetic anisotropy in order to take advantage of the giant magnetostriction at low fields^[7-10]. Newnham^[11] firstly credits the spin reorientation boundary of (Tb-Dy)Fe₂ as a magnetic equivalent to the morphotropic phase boundary (MPB) of a quasi-binary ferroelectric solid solution, i.e., the ferromagnetic MPB, which has been confirmed by Yang *et al.*^[12] and Bergstrom *et al.*^[13]. While the ferromagnetic MPB has demonstrated utility as a design approach for achieving highly sensitive magnetoelastic responses, the predominant focus in current research has been on materials exhibiting a rhombohedral structure, exemplified by Tb_{0.3}Dy_{0.7}Fe₂ (Terfenol-D)^[13,14]. This is because of the highly anisotropic magnetostriction λ_{111} in the pre-transitional rhombohedral side of ferromagnetic MPB, in which giant magnetostriction could be induced by movement of non- 180° domain walls or rotation of magnetic moments^[1,14-16].

As is well known, the magnetization of the rhombohedral (Tb-Dy)Fe₂ domains is expected to distribute equally along one of the eight $\langle 111 \rangle$ easy axes, as shown in Figure 1. The magnetostriction “jump” effect is primarily attributed to the motions of 109° and 71° domain walls under applied magnetic fields^[17-19], although the underlying internal mechanism remains unclear. Several phenomenological approximations, such as domain wall motion and magnetization rotation models, have been proposed to elucidate the magneto-mechanical behaviors of Terfenol-D^[8,20-23]. However, the prevailing mechanisms largely overlook the presence of internal magnetic (stress) fields and assume that each domain evolves independently, which means no magnetic and elastic long-range interactions among domains are considered. Furthermore, the inherent stress resulting from elastic incompatibility in domain walls is of considerable significance, particularly in the case of giant magnetostrictive materials with large intrinsic strain. Since Khachaturyan’s microelasticity theory^[24] was introduced into the phase-field method, it has emerged as a robust technique for simulating the mesoscale microstructural evolution of ferroelectric systems^[25-28]. Zhang *et al.* have proposed a phase-field model that integrates the Khachaturyan microelasticity theory with micromagnetic simulation, enabling the prediction of domain structure stability and temporal evolution^[29]. Subsequently, comparable micromagnetic microelastic phase-field models have been developed to explore domain evolution and magnetoelastic response in proximity to the ferromagnetic MPB^[15,16,30,31].

In this work, the micromagnetic microelastic phase-field method was employed to study the formation and evolution of domains in (Tb-Dy)Fe₂ single crystals within the rhombohedral phase region of the ferromagnetic MPB. Particular emphasis was placed on the two distinct categories of domain walls, namely 71° and 109° domain walls. In the case of the 71° domain wall, the application of an external magnetic field below the coercive field leads to the observation of a domain wall broadening effect, while exceeding the coercive field results in domain switching. Additionally, the applied external magnetic field in the $[100]$ direction leads to 109° domain walls sweeping, which results in heterogeneous magnetization switching.

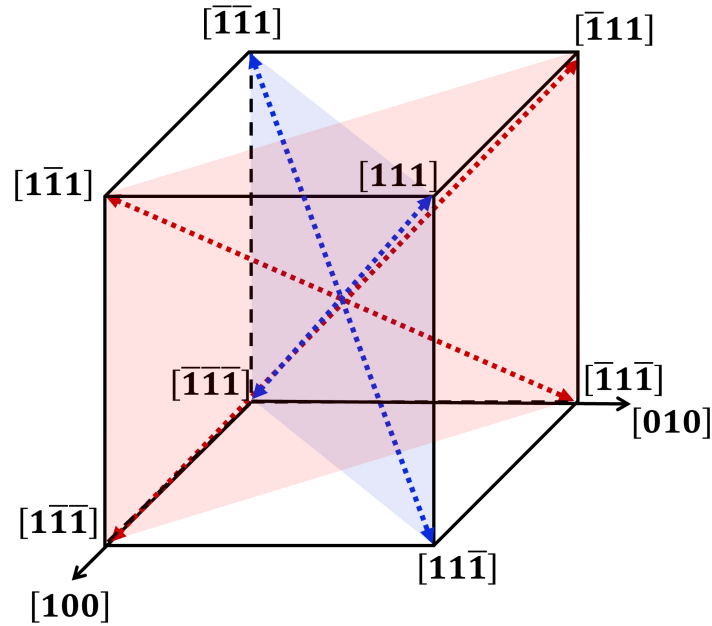


Figure 1. Schematic orientations for eight <111> easy axes in the cubic (Tb-Dy)Fe₂ unit cell.

MATERIALS AND METHODS

The phase-field model employs the local magnetization vector \mathbf{M} (m_1, m_2, m_3) as the primary order parameter, with its spatial distribution representing the magnetic domain microstructure. Therefore, the domain structure can be derived from the time evolution of the local magnetization configuration as governed by the Landau-Lifshitz-Gilbert (LLG) equation, denoted as

$$(1 + \alpha^2) \frac{\partial \mathbf{M}}{\partial t} = -\gamma_0 \mathbf{M} \times \mathbf{H}_{eff} - \frac{\gamma_0 \alpha}{M_s} \mathbf{M} \times (\mathbf{M} \times \mathbf{H}_{eff}) \quad (1)$$

where M_s represents the saturation magnetization, and α and γ_0 denote the damping constant and gyromagnetic ratio, respectively.

The effective magnetic field, denoted as \mathbf{H}_{eff} , is calculated by $\mathbf{H}_{eff} = -(\mu_0 M_s)^{-1} (\delta E_{tot} / \delta \mathbf{m})$ with the vacuum permeability μ_0 and the total free energy E_{tot} . The total free energy, expressed as^[1]

$$E_{tot} = E_{ani} + E_{exc} + E_{ms} + E_{el} + E_{ext} \quad (2)$$

is composed of the magnetocrystalline anisotropy (E_{ani}), exchange (E_{exc}), magnetostatic (E_{ms}), elastic (E_{el}), and external energy (E_{ext}).

The magnetocrystalline anisotropy energy can be defined as^[20,32]

$$E_{ani} = \iiint_V [K_1 (m_1^2 m_2^2 + m_2^2 m_3^2 + m_3^2 m_1^2) + K_2 m_1^2 m_2^2 m_3^2] dV \quad (3)$$

where K_1 and K_2 represent the magnetocrystalline anisotropy coefficients, and V indicates the total volume of the system.

The exchange energy is determined solely by the spatial variation of the magnetization direction and can be written as^[29]

$$E_{exc} = A \int (m_{1,1}^2 + m_{1,2}^2 + m_{1,3}^2 + m_{2,1}^2 + m_{2,2}^2 + m_{2,3}^2 + m_{3,1}^2 + m_{3,2}^2 + m_{3,3}^2) dV \quad (4)$$

where spatial differentiation is denoted by a comma and A is the exchange stiffness constant.

The magnetostatic energy of a system can be denoted as^[29,33]

$$E_{ms} = -\frac{1}{2} \mu_0 M_s \int \mathbf{H}_d \cdot \mathbf{m} dV \quad (5)$$

where \mathbf{H}_d represents the stray field resulting from the long-range interaction between magnetic moments within the system. In the context of a periodic boundary condition, the simulation system is conceptualized as a repetitive building block within 3-D space, and the stray field can be expressed as

$$\mathbf{H}_d = -\nabla\phi + \mathbf{N}_D \bar{\mathbf{M}} \quad (6)$$

where \mathbf{N}_D is the demagnetizing factor dependent solely on the sample's shape. Additionally, $\bar{\mathbf{M}}$ signifies the average magnetization of the simulation system, and ϕ represents the magnetic scalar potential solved utilizing the Fourier spectral method under periodic boundary conditions.

The elastic energy resulting from local deformation can be given as^[20,24,34]

$$E_{el} = \iiint_V \frac{1}{2} c_{ijkl} e_{ij} e_{kl} dV = \int_V \frac{1}{2} c_{ijkl} (\varepsilon_{ij} - \varepsilon_{ij}^0) (\varepsilon_{kl} - \varepsilon_{kl}^0) dV \quad (7)$$

where c_{ijkl} represents the elastic stiffness tensor, e_{ij} denotes the elastic strain, ε_{ij} signifies the total strain, and ε_{ij}^0 indicates the stress-free strain. In cubic magnetostrictive materials, the stress-free strain refers to the spontaneous lattice deformation associated with local magnetization and is denoted by

$$\varepsilon_{ij}^0 = \begin{cases} \frac{3}{2} \lambda_{100} \left(m_i m_j - \frac{1}{3} \right) & (i = j) \\ \frac{3}{2} \lambda_{111} m_i m_j & (i \neq j) \end{cases} \quad (8)$$

Where λ_{100} and λ_{111} are the magnetostrictive constants. Khachaturyan's elastic theory^[24] posits that the total strain ε_{ij} can be expressed as the sum of homogeneous strain $\bar{\varepsilon}$ and heterogeneous strain ε_{ij}^{het} , i.e., $\varepsilon_{ij} = \bar{\varepsilon} + \varepsilon_{ij}^{het}$. The heterogeneous strain adheres to an integral relationship, denoted as $\iiint_V \varepsilon_{ij}^{het} dV = 0$. The equilibrium heterogeneous strain satisfies the mechanical equilibrium condition outlined by the Euler equation for elastic displacement, given as

$$\sigma_{ij,j} = 0 \quad (9)$$

where the stress component σ_{ij} is calculated using

$$\sigma_{ij} = c_{ijkl} e_{kl} (\varepsilon_{kl} - \varepsilon_{kl}^0) \quad (10)$$

Given the assumption of elastic equilibrium at each evolutionary step, the strain and stress values are determined by solving the mechanical equilibrium equation $\nabla \cdot \sigma = 0$ using a Fourier spectral method derived from Khachatryan's elasticity theory^[24]. When a system is exposed to a homogeneous applied stress σ_{ij}^a , the total potential energy is denoted as $E_p = E_{el} - \int_V \sigma_{ij}^a \bar{\varepsilon}_{ij} dV$. Furthermore, the competition between stress-induced anisotropy and magnetic crystal anisotropy has the potential to influence the magnetization behavior of the material^[35].

The external energy resulting from the influence of an externally applied magnetic field, denoted as H_{ex} , can be established as^[36]

$$E_{ext} = -\mu_0 M_s \int \mathbf{H}_{ex} \cdot \mathbf{m} dV \quad (11)$$

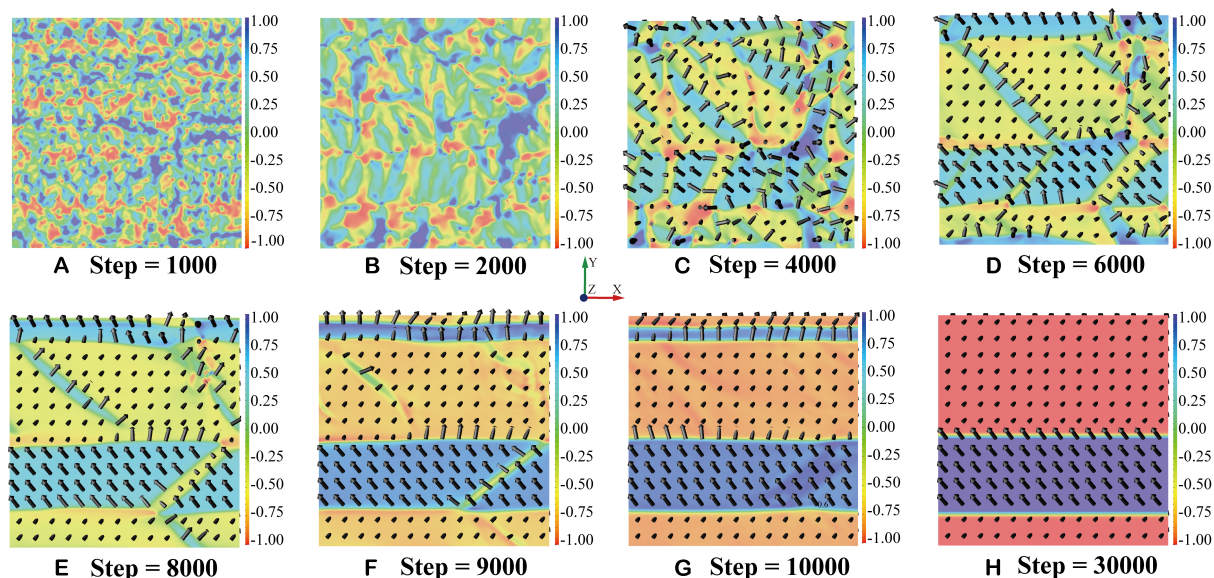
The LLG equation is employed to elucidate the progression of domain microstructure, and its numerical solution is achieved through the Gauss-Seidel projection method^[37]. The simulation focuses on the representative rhombohedral ferromagnetic single system, utilizing material parameters derived from a combination of experimental data and theoretical computations conducted previously^[1,38-41], as outlined comprehensively in [Table 1](#). [Figure 1](#) provides a schematic illustration of the unit cell of (Tb-Dy)Fe₂, which is cubic. The process of domain formation was simulated using the phase-field method, with a dimension of $512\Delta x \times 512\Delta x \times 1\Delta x$. (The 3D phase-field simulation of the domain formation process can be seen in [Supplementary Figure 1](#) in [Supplementary Materials](#)) The simulation grid Δx is 2 nm, smaller than the exchange length $l_{ex} = \sqrt{\frac{2A}{\mu_0 M_s^2}} \approx 4.7 \text{ nm}$ ^[42]. A periodic boundary condition that accommodates non-zero strain is imposed along the three coordinate axes.

RESULTS AND DISCUSSION

[Figure 2](#) illustrates the evolution of domain formation within a representative volume element of the rhombohedral ferromagnetic single crystal, guided by energy minimization towards equilibrium. The initial state is characterized by a random distribution of magnetization, devoid of any predetermined assumptions. The local energy minimum, in conjunction with the presence of inhomogeneous internal stress, serves as the driving force for the initiation nucleation and subsequent growth of various domains. (The distribution of stress during the domain formation process can be seen in [Supplementary Figure 2](#) in [Supplementary Materials](#)). At the early stage, metastable rhombohedral and tetragonal variants function as intermediates, providing low-energy kinetic pathways to final engineered domain configurations. Similar bridging domain mechanism was also identified in previous works^[16,31]. Subsequently, the tetragonal variants gradually disappear as the studied component is in the rhombohedral phase side. In the rhombohedral variants intermediate stages, as shown in [Figure 2D](#) and [E](#), the domains of the rhombohedral phase form twins of either {100} or {110} twin planes, where the twin boundaries are 109° and 71° ferroelectric domain walls, respectively. As the evolution of rhombohedral domains progresses, there is a gradual disappearance

Table 1. The material parameters of (Tb-Dy)Fe₂ in the work

Parameters	Value	Units
Saturation magnetization M_s	8×10^5	A/m
First-order anisotropy coefficient K_1	-6×10^4	J/m ³
Second-order anisotropy coefficient K_2	-2×10^5	J/m ³
Exchange constant A	9×10^{-12}	J/m
Elastic stiffness c_{11}	1.41×10^{11}	N/m ²
Elastic stiffness c_{12}	6.48×10^{10}	N/m ²
Elastic stiffness c_{44}	4.87×10^{10}	N/m ²
Magnetostrictive constant λ_{111}	1,640	ppm
Magnetostrictive constant λ_{100}	100	ppm

**Figure 2.** Domain formation process of the rhombohedral (Tb-Dy)Fe₂ single crystal. The colors correspond to the intensity of magnetization along the z direction, while the black arrows indicate the orientations of magnetization.

of 71° domain walls, ultimately resulting in the survival of two 109° domain walls in the final equilibrium state. It is worth noting that Figure 2H just depicts one of the ideal states of global energy minimization. For the (Tb-Dy)Fe₂ single crystals, 71° and 109° domain walls usually coexist to form complex multi-domain patterns, which collectively affect the magnetoelastic response. To gain deeper insights into the features of both domain walls and their implications for the properties of rhombohedral ferromagnetic single crystals, the detailed evolution behavior of these domain walls under magnetic fields oriented along the $[\bar{1}\bar{1}0]$ and $[100]$ directions have been investigated.

We first study the evolution of the 71° domain wall below the coercive field. As shown in Figure 3, the initial configuration of the simulation is a domain structure containing four 71° domain walls, which consist of $[111]$ and $[11\bar{1}]$ rhombohedral twins. The periodic triangular wave magnetic field with a peak value of 30 kA/m is applied, paralleling the $[\bar{1}\bar{1}0]$ direction. In order to illustrate the detailed evolution of the domain wall, we magnify any of the 71° domain walls in the display. The average magnetization along $[110]$ and $[001]$ directions, denoted as $M_{[110]}$ and $M_{[001]}$, respectively, are also plotted in Figure 3. When the applied

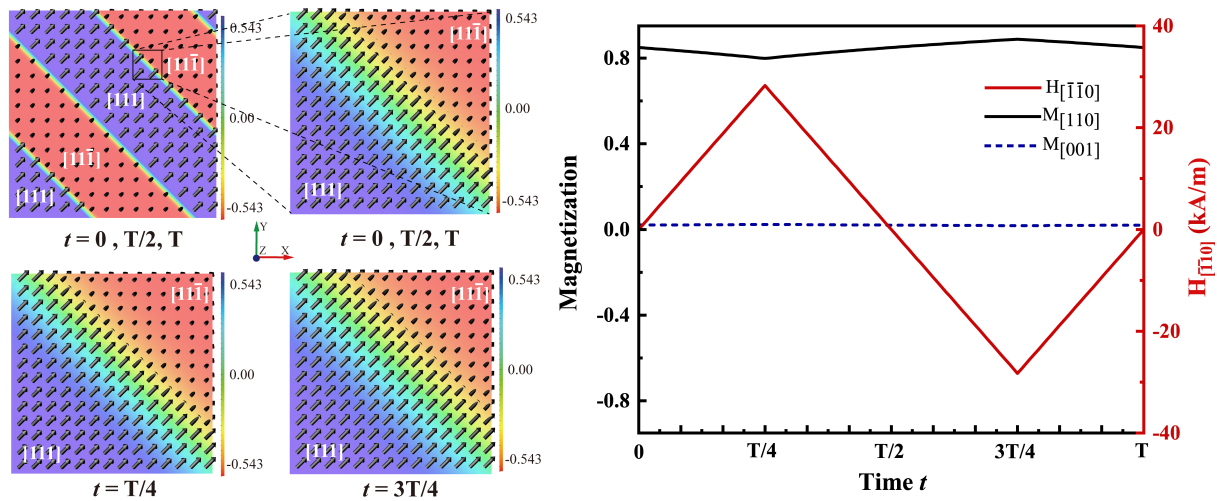


Figure 3. The broadening effect of the 71° domain walls occurs when the applied magnetic field is below the coercive field. The domain wall is magnified to illustrate the fluctuations in its thickness.

magnetic field increases along $[\bar{1}\bar{1}0]$ direction, which is opposite to the magnetization, the 71° domain wall becomes narrower, as shown from $t = 0$ to $t = T/4$. When the applied magnetic field increases along $[110]$ direction, which is in the same direction of the magnetization, the 71° domain wall becomes wider, as shown from $t = T/2$ to $t = 3T/4$. The domain walls reach their maximum thickness ($t = T/4$) and minimum thickness ($t = 3/4 T$) as the field approaches the positive and negative peaks, respectively. The magnetic field dependence of $M_{[110]}$ also demonstrates the narrowing and broadening of the 71° domain walls. Specifically, there is no domain switching throughout the whole process. The value of $M_{[001]}$ stays constant, indicating that the center of 71° domain walls remains motionless.

Magnetization switching is observed upon surpassing the coercive field, as depicted in [Figure 4](#). When the applied magnetic field in the $[\bar{1}\bar{1}0]$ direction increases and surpasses the coercive field, the $M_{[110]}$ value transitions to a negative state, accompanied by the $[111]$ and $[1\bar{1}\bar{1}]$ domains switching to the $[\bar{1}\bar{1}1]$ and $[\bar{1}\bar{1}\bar{1}]$ domains. At $t = T/2$, as the applied field diminishes to zero, the $[\bar{1}\bar{1}1]$ and $[\bar{1}\bar{1}\bar{1}]$ domains are stable. When the applied magnetic field in the reverse direction ($[110]$ direction) surpasses the coercive field, $M_{[110]}$ undergoes a positive jump, accompanied by the $[\bar{1}\bar{1}1]$ and $[\bar{1}\bar{1}\bar{1}]$ domains switching to the $[111]$ and $[11\bar{1}]$ domains. As the reverse applied field decreases to zero at $t = T$, the $[111]$ and $[11\bar{1}]$ domains are stable. In particular, as shown in the dashed line boxes in [Figure 4](#), the significant fluctuation observed in the $M_{[001]}$ curve indicates the complex domain switching (the domain switching can be seen in [Supplementary Figures 3 and 4](#) in [Supplementary Materials](#)), which is different from the homogeneous polarization switching observed in ferroelectric domains^[43]. The magnetic domain switching near $t = T/4$ and $t = 3T/4$ additionally induces a sudden alteration in the magnetostriction of the single crystal (the magnetostriction can be seen in [Supplementary Figure 5](#) in [Supplementary Materials](#)). Throughout the aforementioned domain switching, the position of the 71° domain walls remains constant.

[Figure 5](#) shows magnetic field dependence of the 109° domain wall, which consists of $[11\bar{1}]$ and $[\bar{1}11]$ rhombohedral twins. At step = 0, a constant magnetic field of 20 kA/m is promptly applied along the $[100]$ direction. Under the applied magnetic field, the favored $[11\bar{1}]$ domain expands, displacing the 109° domain

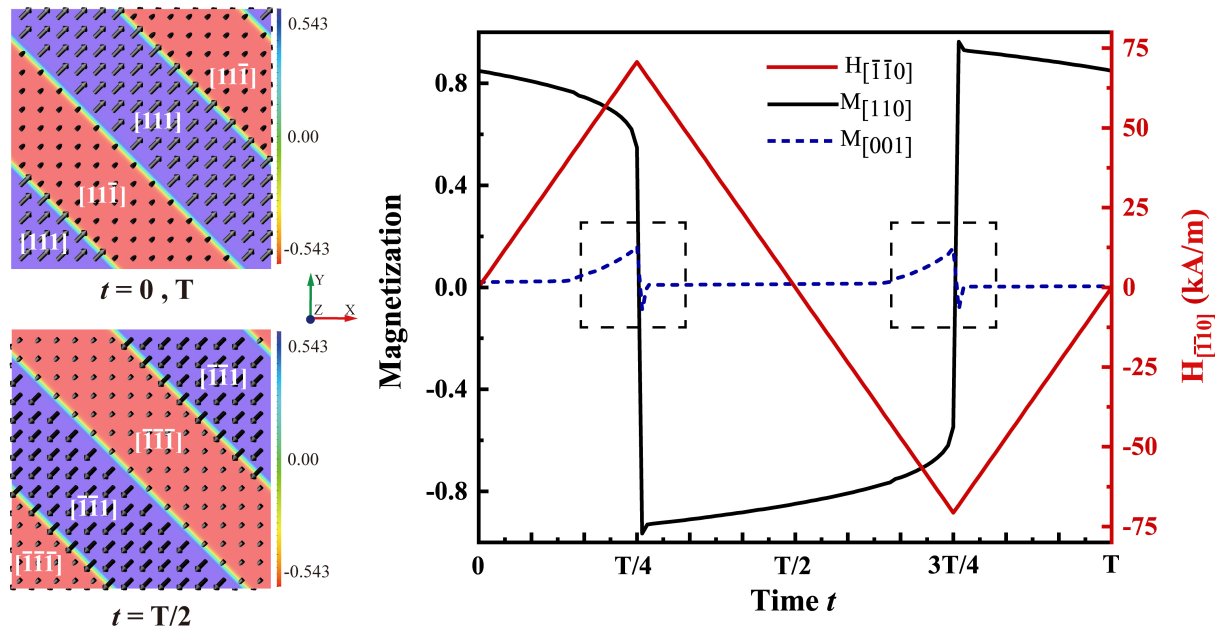


Figure 4. Magnetization switching occurs upon surpassing the coercive field. The domains before and after switching are depicted on the left.

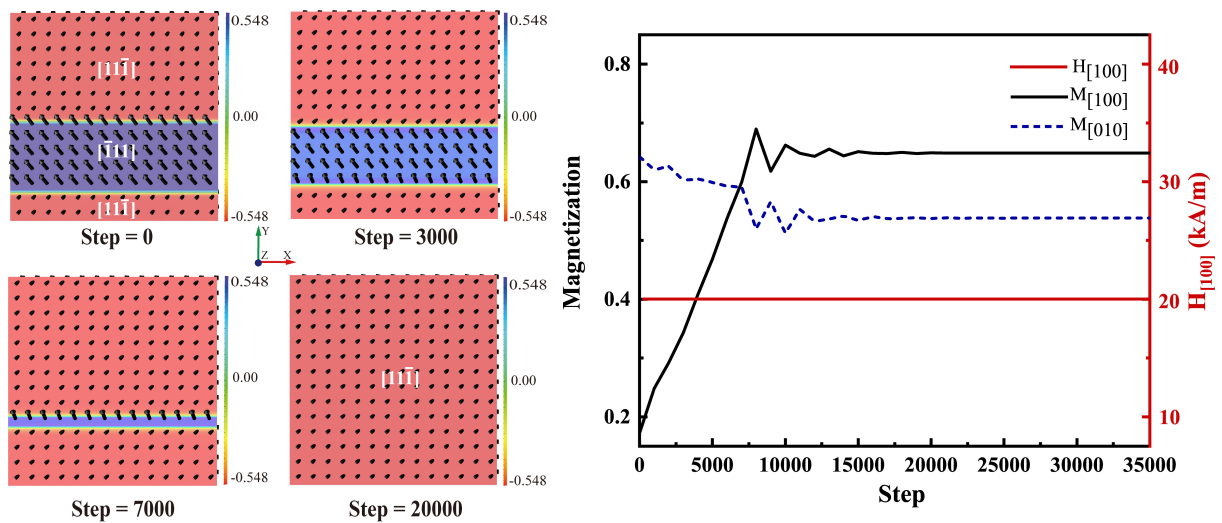


Figure 5. The moving of 109° domain walls and the occurrence of heterogeneous magnetization switching in response to a constant magnetic field of 20 kA/m. The merging and disappearance of two domain walls resulted in the formation of a single domain.

walls towards the disfavored $[1\bar{1}\bar{1}]$ domain. The $M_{[100]}$ gradually increases from the beginning to step = 7,000, corresponding to the linear movement of 109° domain walls. After that, the curves of $M_{[100]}$ and $M_{[010]}$ vibrate violently and remain at constant values. This phenomenon arises due to the convergence and subsequent merger of the two 109° domain walls, leading to their eventual disappearance. The $[1\bar{1}\bar{1}]$ domain undergoes a complete transition to $[11\bar{1}]$, facilitated by the movement of the 109° domain walls, resulting in the formation of a single magnetic domain. Heterogeneous strain occurs in the domain switching process to accommodate the local deformations. If zero-strain periodic boundary conditions are implemented, the

mechanical clamping effect prevents the merging of the two 109° domain walls, thereby inhibiting the formation of a single magnetic domain. It is important to acknowledge that the slower movement of the 109° domain wall can also be induced by applying fields (2 kA/m for example) significantly lower than those examined in this study. (The 109° magnetic domain walls move fast under the magnetic field exceeding 20 kA/m, as shown in [Supplementary Figure 6](#)). This implies the absence of a critical magnetic field necessary to induce the displacement of 109° domain walls. This occurs because the $[11\bar{1}]$ domain is favored by the $[100]$ applied field, whereas the $[\bar{1}11]$ domain is in the disfavored region with higher energy. The two domain regions compete to drive the 109° domain wall in between from the favored domain region to the disfavored one. Generally, this local heterogeneous domain switching can be used in domain engineering^[16] to tailor the magnetic domain morphology with enhanced magnetostrictive properties.

CONCLUSIONS

This study utilized micromagnetic microelastic modeling through the phase-field method to investigate the process of domain formation and the evolution of domain walls in (Tb-Dy)Fe₂ single crystals situated in the vicinity of the rhombohedral region of the ferromagnetic MPB. Particular emphasis was placed on the 71° and 109° domain walls, as their alterations in domain structure under applied magnetic field are crucial to the magnetelastic response of giant magnetostrictive materials. In the case of low applied magnetic field, a phenomenon of domain wall broadening was noted on the 71° domain walls, whereas in the case of high applied magnetic field, homogeneous magnetization switching took place without any observable movement of domain walls. The magnetization switching also helps understand the magnetostriction "jump" effect of the rhombohedral single crystal. The act of sweeping the 109° domain walls resulted in the occurrence of heterogeneous magnetization switching through the movement of domain walls. The detailed analysis of the two domain evolution mechanisms provided insightful understanding into the engineered domain structures of rhombohedral (Tb-Dy)Fe₂ single crystals. Furthermore, these findings offer valuable guidance for the future design of magnetostrictive materials through domain engineering.

DECLARATIONS

Authors' contributions

Conception and design of the study: Hu CC, Zhang Z, Xu YX

Data analysis and interpretation: Xu YX, Hu CC, Dong SZ, Huang HH, Li W

Manuscript writing and revising: Xu YX, Cai TT, Hu CC, Zhang Z, Li W

Simulation guide: Huang HB, Rao WF, Chen LQ

Supervision: Hu CC, Zhang Z, Rao WF

Availability of data and materials

The data that support the findings of this study are available from the corresponding author upon reasonable request.

Financial support and sponsorship

This work was financially supported by the National Natural Science Foundation of China (No. 52301088), the Science Foundation of Shandong Province, China (No. ZR2022ME030 and No. ZR2020QE028), the National Natural Science Foundation of China (No. 12204215 and No. 12174210), the Research Foundation of Liaocheng University (No. 318012119). Chen LQ is the owner of Mu-PRO LLC, which licensed the computer codes for generating the phase-field results from the Penn State Research Foundation.

Conflicts of interest

Chen LQ is the owner of Mu-PRO LLC, which licensed the computer codes for generating the phase-field results from the Penn State Research Foundation, while the other authors have declared that they have no conflicts of interest.

Ethical approval and consent to participate

Not applicable.

Consent for publication

Not applicable.

Copyright

© The Author(s) 2024.

REFERENCES

1. Clark AE. Handbook of ferromagnetic materials. In: Wohlfarth EP, editor. Magnetostrictive rare earth-Fe₂ compounds. Amsterdam: North-Holland; 1980. pp. 531-89.
2. Liu J, Jiang C, Xu H. Giant magnetostrictive materials. *Sci China Technol Sci* 2012;55:1319-26. DOI
3. Zhou SZ, Gao XX. Magnetostrictive materials. Beijing: Metallurgical Industry Press; 2017.
4. Yu C, Niu R, Peng Z, et al. A current sensor based on capillary microresonator filled with terfenol-D nanoparticles. *IEEE Photon Technol Lett* 2021;33:239-42. DOI
5. Liu C, Shen T, Feng Y, Liu H, Han W. First-principles calculations to investigate electronic, magnetism, elastic properties of Tb_xDy_{1-x}Fe₂ (x = 0, 0.25, 0.5, 1). *J Magn Magn Mater* 2022;547:168953. DOI
6. Tu S, Mai Y, Tong Y, Liu T, Dong M, Wang Q. Enhancement of magnetostrictive performance of Tb_{0.27}Dy_{0.73}Fe_{1.95} by solidification in high magnetic field gradient. *J Alloys Compd* 2018;741:1006-11. DOI
7. Liu J, Ren W, Li D, et al. Magnetic transitions and magnetostrictive properties of Tb_xDy_{1-x}(Fe_{0.8}Co_{0.2})₂ (0.20 ≤ x ≤ 0.40). *Phys Rev B* 2007;75:064429. DOI
8. Hu CC, Shi YG, Shi DN, Tang SL, Fan JY, Du YW. Anisotropy compensation and magnetostrictive properties in Tb_xDy_{1-x}(Fe_{0.9}Mn_{0.1})_{1.93} Laves compounds: experimental and theoretical analysis. *J Appl Phys* 2013;113:203906. DOI
9. Zhou Z, Li J, Bao X, Liu M, Gao X. Improvement of mechanical properties of magnetostrictive Tb-Dy-Fe alloys via preparing sintered material with low-melting Dy-Cu alloy binder. *J Alloys Compd* 2022;895:162572. DOI
10. Dong M, Liu T, Guo X, Liu Y, Dong S, Wang Q. Enhancement of mechanical properties of Tb_{0.27}Dy_{0.73}Fe_{1.95} alloy by directional solidification in high magnetic field. *Mater Sci Eng A* 2020;785:139377. DOI
11. Newnham RE. Phase transformations in smart materials. *Acta Cryst* 1998;54:729-37. DOI
12. Yang S, Bao H, Zhou C, et al. Large magnetostriction from morphotropic phase boundary in ferromagnets. *Phys Rev Lett* 2010;104:197201. DOI
13. Bergstrom R Jr, Wuttig M, Cullen J, et al. Morphotropic phase boundaries in ferromagnets: Tb_{1-x}Dy_xFe₂ alloys. *Phys Rev Lett* 2013;111:017203. DOI
14. Hu C, Zhang Z, Cheng X, Huang H, Shi Y, Chen L. Ultrasensitive magnetostrictive responses at the pre-transitional rhombohedral side of ferromagnetic morphotropic phase boundary. *J Mater Sci* 2021;56:1713-29. DOI
15. Ke X, Zhou C, Tian B, et al. Direct evidence of magnetization rotation at the ferromagnetic morphotropic phase boundary in Tb_{1-x}Dy_xFe₂ system. *Phys Rev B* 2023;108:224419. DOI
16. Xu Y, Wu Y, Hu C, et al. Domain engineering in ferromagnetic morphotropic phase boundary with enhanced and non-hysteretic magnetostriction: a phase-field simulation. *Scr Mater* 2024;242:115916. DOI
17. Wang B, Busbridge S, Li Y, Wu G, Piercy A. Magnetostriction and magnetization process of Tb_{0.27}Dy_{0.73}Fe₂ single crystal. *J Magn Magn Mater* 2000;218:198-202. DOI
18. Galloway N, Schulze MP, Greenough RD, Jiles DC. Enhanced differential magnetostrictive response in annealed Terfenol-D. *Appl Phys Lett* 1993;63:842-4. DOI
19. Zhao Y, Jiang C, Zhang H, Xu H. Magnetostriction of <110> oriented crystals in the TbDyFe alloy. *J Alloys Compd* 2003;354:263-8. DOI
20. Jiles D, Thoeke J. Theoretical modelling of the effects of anisotropy and stress on the magnetization and magnetostriction of Tb_{0.3}Dy_{0.7}Fe₂. *J Magn Magn Mater* 1994;134:143-60. DOI
21. Desimone A, James RD. A theory of magnetostriction oriented towards applications. *J Appl Phys* 1997;81:5706-8. DOI
22. Zhao X, Lord D. Effect of demagnetization fields on the magnetization processes in Terfenol-D. *J Magn Magn Mater* 1999;195:699-707. DOI
23. Armstrong WD. An incremental theory of magneto-elastic hysteresis in pseudo-cubic ferro-magnetostrictive alloys. *J Magn Magn*

- Mater* 2003;263:208-18. DOI
24. Khachaturyan AG. Theory of structural transformation in solids. New York: Wiley; 1983.
 25. Choudhury S, Li Y, Krilliii C, Chen L. Phase-field simulation of polarization switching and domain evolution in ferroelectric polycrystals. *Acta Mater* 2005;53:5313-21. DOI
 26. Ke X, Wang D, Ren X, Wang Y. Polarization spinodal at ferroelectric morphotropic phase boundary. *Phys Rev Lett* 2020;125:127602. DOI PubMed
 27. Rao W, Wang YU. Domain wall broadening mechanism for domain size effect of enhanced piezoelectricity in crystallographically engineered ferroelectric single crystals. *Appl Phys Lett* 2007;90:041915. DOI
 28. Guo C, Huang H. Design of super-elastic freestanding ferroelectric thin films guided by phase-field simulations. *Microstructures* 2022;2:2022021. DOI
 29. Zhang J, Chen L. Phase-field microelasticity theory and micromagnetic simulations of domain structures in giant magnetostrictive materials. *Acta Mater* 2005;53:2845-55. DOI
 30. Huang YY, Jin YM. Phase field modeling of magnetization processes in growth twinned Terfenol-D crystals. *Appl Phys Lett* 2008;93:142504. DOI
 31. Hu C, Yang T, Huang H, et al. Phase-field simulation of domain structures and magnetostrictive response in Tb_{1-x}Dy_xFe₂ alloys near morphotropic phase boundary. *Appl Phys Lett* 2016;108:141908. DOI
 32. Yang YV, Huang YY, Jin YM. Effects of magnetocrystalline anisotropy constant K₂ on magnetization and magnetostriction of Terfenol-D. *Appl Phys Lett* 2011;98:012503. DOI
 33. Hu J, Nan CW. Electric-field-induced magnetic easy-axis reorientation in ferromagnetic/ferroelectric layered heterostructures. *Phys Rev B* 2009;80:224416. DOI
 34. Stroh AN. Steady state problems in anisotropic elasticity. *J Math Phys* 1962;41:77-103. DOI
 35. Sun Z, Li L, Yang G, Wang L. Micromagnetic simulation of Nd-Fe-B demagnetization behavior in complex environments. *J Magn Mater* 2024;589:171555. DOI
 36. Armstrong WD. Burst magnetostriction in Tb_{0.3}Dy_{0.7}Fe_{1.9}. *J Appl Phys* 1997;81:3548-54. DOI
 37. Wang XP, García-Cervera CJ, E W. A gauss-seidel projection method for micromagnetics simulations. *J Comput Phys* 2001;171:357-72. DOI
 38. Clark A, Savage H, Spano M. Effect of stress on the magnetostriction and magnetization of single crystal Tb_{0.27}Dy_{0.73}Fe₂. *IEEE Trans Magn* 1984;20:1443-5. DOI
 39. Wang BL, Jin YM. Magnetization and magnetostriction of Terfenol-D near spin reorientation boundary. *J Appl Phys* 2012;111:103908. DOI
 40. Martin KN, de Groot PAJ, Rainford BD, et al. Magnetic anisotropy in the cubic Laves REFe₂ intermetallic compounds. *J Phys Condens Matter* 2006;18:5861-71. DOI
 41. Shu Y, Lin M, Wu K. Micromagnetic modeling of magnetostrictive materials under intrinsic stress. *Mech Mater* 2004;36:975-97. DOI
 42. Abo GS, Hong Y, Park J, Lee J, Lee W, Choi B. Definition of magnetic exchange length. *IEEE Trans Magn* 2013;49:4937-9. DOI
 43. Lv P, Lynch CS. Phase-field simulation of domain walls in rhombohedral ferroelectric single crystals. *Acta Mater* 2018;155:245-52. DOI